Plasma Sci. Technol. **19** (2017) 045603 (8pp) https://doi.org/10.1088/2058-6272/aa4ee0

Modelling of carbon erosion and re-deposition for the EAST movable limiter*

Hai XIE (谢海)[1], Rui DING (丁锐)[1,3], Junling CHEN (陈俊凌)[1] and Jizhong SUN (孙继忠)[2]

[1] Institute of Plasma Physics, Chinese Academy of Sciences, Hefei 230021, People's Republic of China
[2] School of Physics and Optoelectronic Technology, Dalian University of Technology, Dalian 116024, People's Republic of China

E-mail: rding@ipp.ac.cn

Received 21 July 2016, revised 17 November 2016
Accepted for publication 21 November 2016
Published 9 March 2017

Abstract

The movable limiter at the mid-plane of the Experimental Advanced Superconducting Tokamak (EAST) with carbon coatings on the surface was exposed to edge plasma to study the material erosion and re-deposition. After the experiments, the carbon erosion and re-deposition is modelled using the 3D Monte Carlo code ERO. The geometry of the movable limiter, 3D configuration of the plasma parameters and electromagnetic fields under both limiter and divertor configurations have been implemented into the code. In the simulations, the main uncertain parameters such as carbon concentration ρ_c in the background plasma and cross-field transport coefficient $D_\perp$ in the vicinity of surface according to the 'funneling model', have been studied in comparison with experiments. The parameter ρ_c mainly influences the net erosion and deposition profiles of the two sides of the movable limiter, while $D_\perp$ mostly changes the profiles on the top surface.

Keywords: modelling, EAST, limiter, erosion and deposition

(Some figures may appear in colour only in the online journal)

1. Introduction

The plasma–wall interaction (PWI) is one of the key issues for material choice and plasma scenarios in ITER [1, 2]. The lifetime of plasma facing components (PFCs) is determined by the erosion and deposition processes. Moreover, the eroded materials can migrate over long distances and co-deposit with fuel species back to the wall. For operations with tritium, the build-up of tritium-rich layers could lead to safety issues due to its high radioactivity [3]. Therefore, it is crucial to understand the processes of material erosion, impurity transport and re-deposition in fusion devices, and make more precise predictions for the next generation devices, such as ITER.

For the plasma start-up and ramp-down for ITER, it was initially supposed to use two symmetric start-up beryllium limiters at the low field side to handle the power and particle fluxes [4]. As the limiter phase is very short, erosion is not a critical issue. Therefore, the plasma start-up and ramp-down on the main wall are proposed in the current ITER design [5]. However, the erosion of the first wall in steady state could be very high, as suggested by modelling from different codes [6, 7]. Therefore the modelling codes have to be improved continuously by benchmarking against various existing experiments for a better description of reality. Experiments have been carried out on the Experimental Advanced Superconducting Tokamak (EAST) in which the movable limiter (ML) with four carbon-coated tiles was exposed to the scrape-off layer (SOL) plasma. Net erosion can be detected according to the carbon thickness variation before and after the exposure. Since only rough results have been achieved by

* Supported by the National Magnetic Confinement Fusion Science Program of China (Nos. 2013GB107004 and 2013GB105003), National Natural Science Foundation of China (Nos. 11375010, 11675218 and 11005125), and the Sino-German Center for Research Promotion under contract No GZ769.
[3] Author to whom any correspondence should be addressed.

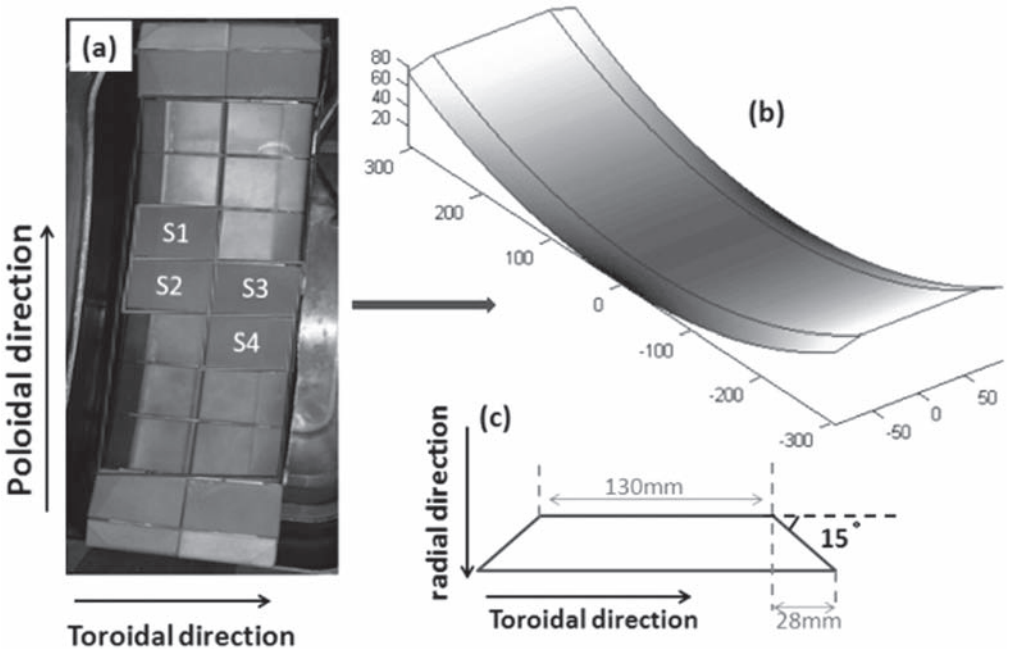

Figure 1. General shape of the movable limiter. (a) Picture of the movable limiter with four tiles (S1, S2, S3, S4) marked with $\sim$1 μm carbon films. (b) 3D shape model of the movable limiter. (c) Toroidal cross-section of the limiter.

the campaign averaged experiments, it is necessary to obtain more detailed information through simulation of erosion and deposition for the limiter.

It is well known that material erosion is of prime importance as the starting point of impurity transport and re-deposition. One of the main parameters determining the erosion rate is the background plasma flux impinging on the material surface, which is often assumed to be due to transport along the magnetic field only. Under this assumption, the particle flux densities received by the surface are close to zero when the magnetic field is nearly parallel to the PFCs. However, experiments performed on different tokamak devices such as DITE [8], HT-7 [9], DIIID [10] and JET [11] indicate that there are substantial fluxes to the surface even at grazing angles of magnetic field. Several previous works have been done [12–15] to address this issue. For the EAST movable limiter, most of the area is nearly tangential to the magnetic field. This paper presents modelling results of the movable limiter exposure experiments using the three dimensional Monte Carlo code ERO [16], which simulates surface erosion, impurity transport and deposition in a given background plasma. The 'funnel effect' [14], which takes into account the perpendicular flux to the surface, is also taken into account in the modelling.

2. Experiments on EAST

EAST was built for long pulse operations over 1000 s with plasma current $I_p \sim 1$ MA, electron temperature $T_e > 10$ keV, and electron density $n_e > 10^{20}$ m^{-3} [17]. It provides a good platform for experiments under steady state conditions. There are two movable limiters (MLs) equipped at EAST low field side (LFS) on P port and G port respectively to control the EAST plasma boundary [18]. The limiter tiles are made of graphite to withstand high thermal power loads and then coated with SiC using the same technique as for all the other graphite plasma facing components in EAST [19]. To reduce heat and particle flux, the geometry of the ML at the poloidal direction is a concave shape so that the angles between the limiter surface and the magnetic surface could be very small. Both sides of the MLs are shaped with tilted angles of about 15° as shown in figure 1(c). The middle top surface of the limiter tiles are flat therefore do not exactly match the toroidal curvature of the magnetic flux surfaces. More details about the ML structure and assembly can be found in [18]. In order to study the material erosion and deposition under steady state conditions, four tiles of one ML (S1, S2, S3 and S4 shown in figure 1(a)) were marked by vapor deposition of 1 nm tungsten and following 1 μm carbon on the top of the surface. After that the ML were exposed to plasma in the 2010 EAST campaign.

During the operation, the radial position of the ML was kept at the position with a major radius of 2.37 m. The movable limiter was subject to strong plasma–surface interactions during the discharges, as shown in figure 2. During the campaign, about two thirds of the total exposure time was in limiter configurations and the remaining one third of the time had divertor configurations. Fast reciprocating Langmuir probes were mounted at the midplane of the port close to the ML for measurements of the boundary plasma conditions, such as the profiles of electron temperature and density. Erosion and deposition of the four marked tiles were detected by Rutherford backscattering spectrometry (RBS) analysis before and after the exposure, and the measured results showed that all 1 μm of the marked carbon films and 1 nm W films were completely removed. Therefore, taking into

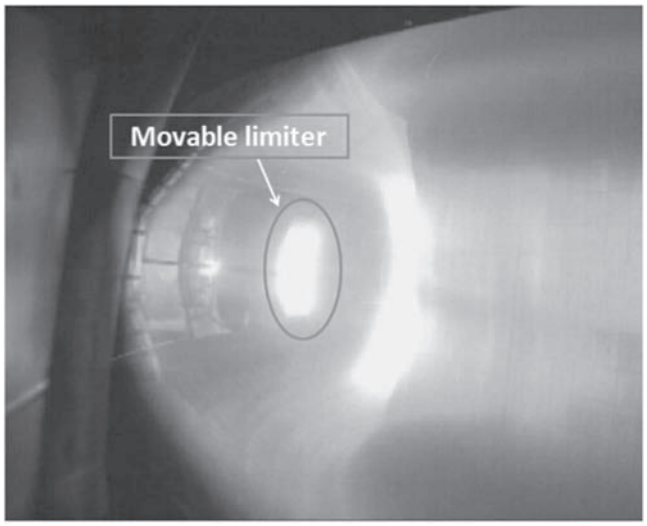

Figure 2. CCD photograph of the EAST vacuum vessel during main discharge. Light emission shows a strong plasma interaction with the movable limiter.

account the total plasma exposure time of about 36 000 s, the campaign averaged carbon net erosion rate is larger than $0.028\ \mathrm{nm\ s^{-1}}$. A simulation was carried out for more detailed analysis of erosion and deposition for the ML. The issues for the shallow impact angles of a magnetic field on the material surface were addressed in the modelling.

3. Modelling with the ERO code

The erosion and deposition of the ML are modelled using the 3D Monte Carlo Code ERO [16], which calculates the erosion of target materials with a given geometry, transport of impurities through a given background plasma and resulting re-deposition of eroded materials. A geometry model for the central part of the ML, without the top and bottom edge structures of the actual ML that are designed to protect the ML, has been implemented into the ERO code, as shown in figures 1(b) and (c). The outline of the limiter geometry in the poloidal direction is an arc with a radius of 680 mm, while in the toroidal direction there are 15° inclined edges with a length of 28 mm at both sides. The poloidal length and toroidal length are 617 mm and 186 mm, respectively.

Because the plasma particle density flux to the surface determines the gross erosion rates of the materials, it is essential to verify the flux model for the simulation. The density flux arriving at the material surface is usually assumed to be only due to parallel transport (along the magnetic field lines) according to the angle between the magnetic field and material surface. Here the angle takes into account the effect of the relative differences in curvatures of the magnetic flux surfaces and the limiter surface, both toroidally and poloidally. Under this assumption the flux decreases and approaches zero when the magnetic field line is nearly parallel to the limiter or at shallow impact angles [14]. However, it has been found that surfaces tangential to the magnetic field lines can receive substantial flux rather than the negligible levels expected by the parallel flux [8–12]. One of the reasons for this issue is the changing of the sheath structure. When the angle between the magnetic field and the surface normal α is larger than $\sim 89°$ for deuterium plasma, it might be expected that the ions reach the wall faster than the electrons because of their larger Larmor radius, and as a result a more complex sheath in front of the wall arises [15]. This leads to more uncertainties for calculating the amount of plasma flux arriving at the material surface. Theoretical analysis of the shallow angle case indicated that there are still fluxes onto the material surface even when the magnetic field is parallel to the wall [12]. Therefore, the perpendicular flux can dominate the overall impinging flux at shallow B field angles. A cut-off angle is usually used in the ERO code such that for larger impact angles the impinging particle flux is kept constant as the value for the cut-off angle.

However, for the EAST movable limiter, all of the top surface areas are in the case of $\alpha > 89°$. Thus, in this simulation, to make a more accurate simulation, a flux model which contains both parallel and perpendicular plasma density flux to the magnetic field has been applied for modelling of the ML top surface. The parallel flux is determined by the plasma density and temperature profiles in the SOL, and decreases exponentially with the radial distance to the last closed flux surface (LCFS) [16]

$$\Gamma_{\parallel} = n_{\mathrm{LCFS}} \exp\left(\frac{-R_{\mathrm{LCFS}}}{\lambda_n}\right) c_{\mathrm{s}} \tag{1}$$

with $c_{\mathrm{s}} = [k(T_{\mathrm{i}} + T_{\mathrm{e}})/m_{\mathrm{i}}]^{1/2}$, where c_{s} is the ion acoustic speed of fuel ions with mass m_{i}, n_{LCFS} the plasma density at the LCFS, R_{LCFS} the radial distance from the limiter surface to the LCFS and λ_n the characteristic scale length for the radial density decay. In the formula, $n_{\mathrm{LCFS}} \exp(-R_{\mathrm{LCFS}}/\lambda_n)$ is the density at the entrance of the sheath close to the limiter surface. Taking into account both parallel and perpendicular flux, the density flux arriving at the surface can be written as

$$\Gamma_{\mathrm{sur}} = \Gamma_{\parallel} \cos\alpha + \Gamma_{\perp} \sin\alpha \tag{2}$$

with α the angle between the surface normal and magnetic field. Note that $\Gamma_{\perp}$ is only taken into consideration for the ML top surface with shallow B field angles ($\alpha > 89°$). For smaller angles, the contribution of $\Gamma_{\perp}$ can be neglected compared to the parallel flux; therefore, the parallel flux plays a dominant role for both sides of the ML because of the B field angles of about 15°. According to Stangeby's 'funneling model' [14], in the vicinity of the surface, the ratio between the perpendicular density flux and the parallel density flux for a surface with shallow angles can be obtained by

$$\Gamma_{\perp}/\Gamma_{\parallel} = (2D_{\perp}/L_f c_{\mathrm{s}})^{1/2} \tag{3}$$

where $2L_f$ is the toroidal width of the ML top surface, and $D_{\perp}$ is the cross field transport coefficient of plasma density. Generally the cross field transport coefficient is anomalous and uncertain.

For most shots in the campaign, the start up and ramp down phases took place at the high field side (HFS) limiter. Therefore the erosion and deposition of the ML in the flat-top phase are considered in the simulation, including two

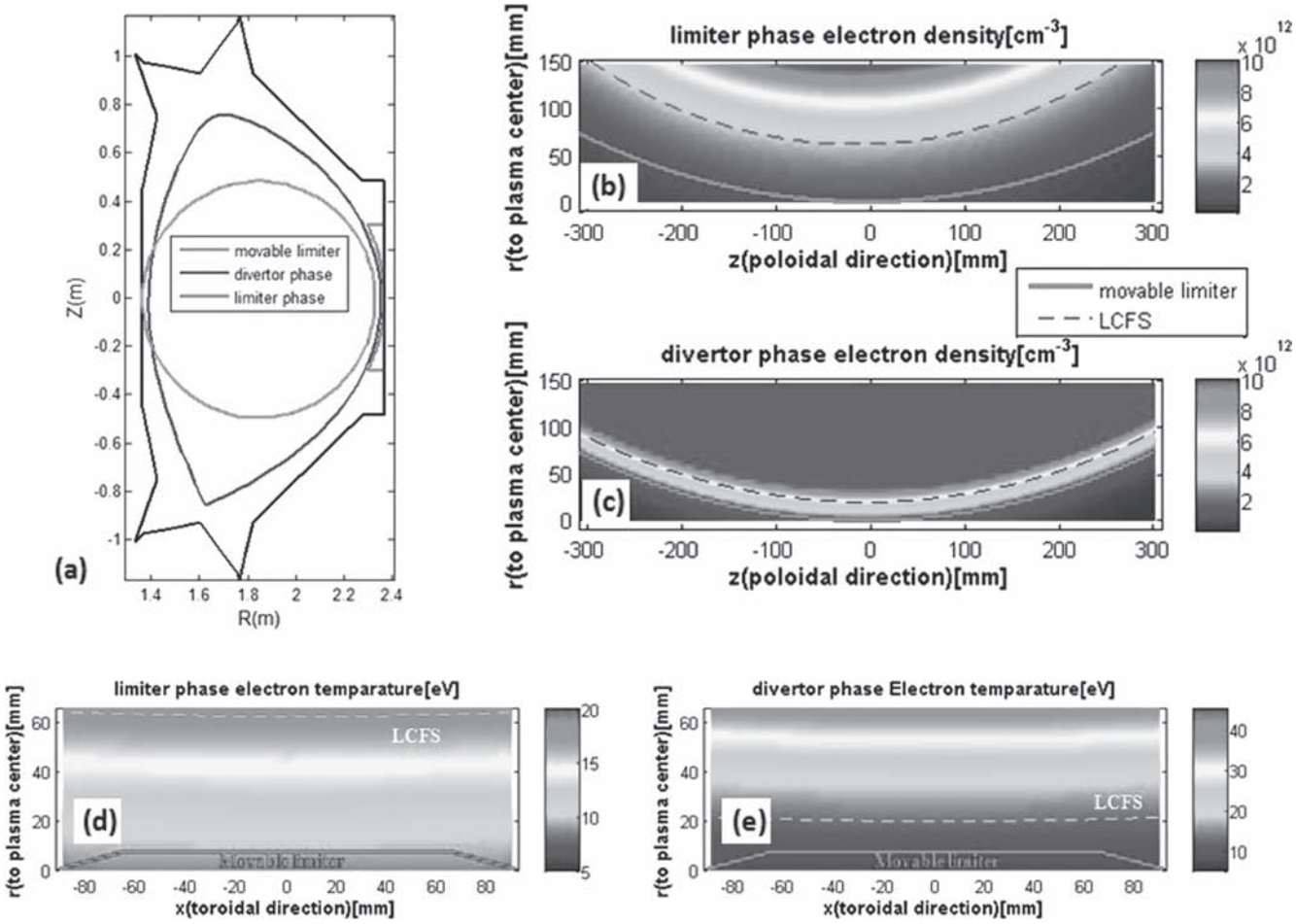

Figure 3. Typical experiment geometry. (a) Poloidal position of the movable limiter and LCFS geometry of the two phases. (b) and (c) Poloidal cross-section of the electron density for the limiter phase and the divertor phase, respectively. (d) and (e) Toroidal cross-section of the electron temperature for the limiter phase and the divertor phase, respectively.

different kinds of configurations of the divertor phase and the limiter phase. The background plasma parameters for the two phases are obtained from two typical shots. The 3D magnetic field geometries can be achieved by equilibrium fitting (EFIT) calculations [20]. Figure 3(a) illustrates the general geometry of the LCFS and the ML. The radial distances to the LCFS from the ML surface at the midplane for the limiter phase and the divertor phase are about 62 mm and 23 mm, respectively. The LCFS curvature radius of the divertor phase is much larger than that of the limiter phase, which results in the relatively different parameter distribution in the poloidal direction. The radial profiles of electron density and temperature in the SOL are taken from measurements with the fast reciprocating Langmuir probe, which are used for the background plasma in the ERO modeling. According to the probe measurements, figures 3(b) and (c) are the poloidal cross-section of the electron density together with the limiter contour for the limiter phase and the divertor phase, respectively. Toroidal symmetry is assumed to obtain the 3D picture just by rotation of the 2D map around the torus axis. The toroidal cross-section of the electron temperature of the limiter phase and the divertor phase are shown in figures 3(d) and (e).

4. Modeling results and discussions

The material erosion, transport and re-deposition for the ML in the two discharge phases are modelled. The eroded impurities originating from the surface are ionized or dissociated and then forced by friction with the background deuterium ion flow. The main plasma flow in the SOL above the ML is in the same direction as the magnetic field, and the flow velocity is increasing and is up to ion acoustic speed c_s when close to the wall surface. The erosion of the carbon is mainly caused by physical sputtering and chemical erosion. The physical sputtering yields for different background species are determined by impact energies and angles. In ERO simulations, the average physical sputtering yield is used according to the Abramov approximation with the assumptions of normal incidence and shifted Maxwellian energy distribution due to the acceleration in the sheath potential [16, 21]. The chemical erosion yield depends not only on the deuterium impact energies, but also on the impinging flux and surface temperature, which can be calculated according to the Roth formula [22]. As the ML surface temperature T has not been measured during plasma exposure, with the assumption of $T = 500$ K and related plasma condition on the ML surface

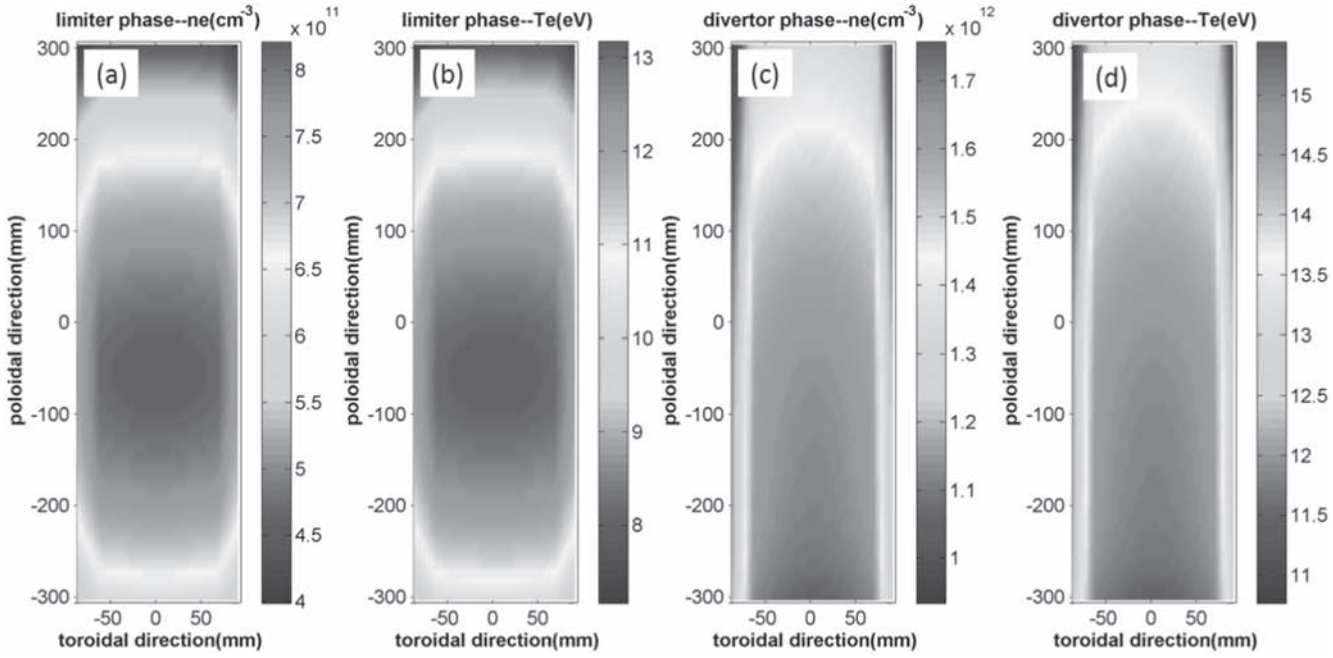

Figure 4. Electron density n_e and electron temperature T_e on the ML surface. (a) n_e in the limiter phase. (b) T_e in the limiter phase. (c) n_e in the divertor phase. (d) T_e in the divertor phase.

(as shown in figure 4), the chemical erosion yield calculated by the Roth formula is about 1.3%–1.7%. Therefore, in the simulations, the chemical erosion yield of a graphite substrate by deuterium bombardment is assumed to be 1.5% according to the previously measured values [23, 24]. It is assumed that only CD_4 molecules are generated in the process of chemical erosion and to have a Maxwellian energy distribution. The break-up of methane into various hydrocarbon species is calculated according to the corresponding reaction rate coefficients [25]. The effective sticking coefficient for hydrocarbon molecules hitting the material surface is another uncertain parameter. According to the previous ERO modelling of local carbon deposition from methane and ethane injection in the TEXTOR tokamak, the effective sticking coefficient can be assumed to be 0.15 [26]. Because the neutral density in the boundary plasma has not yet been measured during the campaign, charge exchange atoms are not considered in the simulation. There are other unknown crucial parameters, such as the carbon concentration in the background plasma and the cross field transport coefficient. These parameters have been studied as stated below.

The carbon impurity concentration (ρ_c) in the background plasma is an important input for the modeling as it influences carbon deposition. The reflection probability coefficient of the impurity is determined by the TRIM code according to the incident energy and angle [16]. As the carbon concentration in the background edge plasma of EAST was not measured, the carbon concentration is assumed to be the same in the modeling for the two configuration cases. In order to compare with the experiments, the modelled erosion and deposition profiles are calculated by superposition of two third of the limiter phase with one third of the divertor phase according to the ratio of the total exposure time, which is the

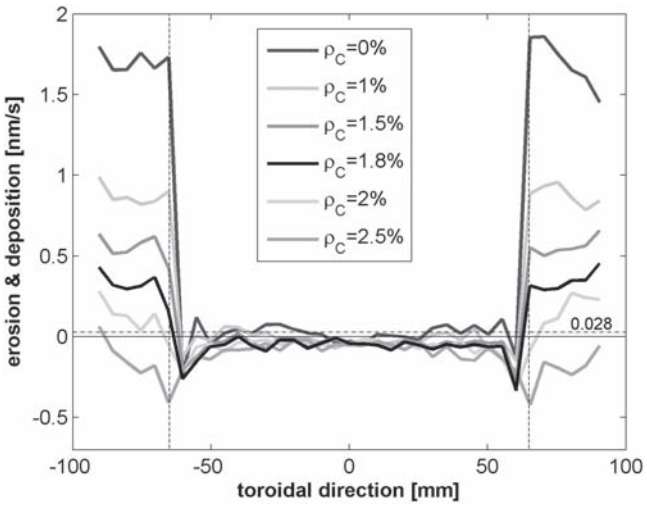

Figure 5. Modelled profiles of erosion and deposition distribution along the toroidal direction at the midplane (poloidal direction $z = 0$) of the movable limiter for different background carbon concentrations (ρ_c) for $D_\perp = 0$. Positive values represent erosion, negative ones deposition.

campaign averaged result. Figure 5 shows the modelled profiles of carbon net deposition and erosion along the ML in the toroidal direction of the midplane with different assumptions of carbon concentration and the assumption of $D_\perp = 0$. The value of the assumed carbon concentration is independent of the radial location. The charge state of carbon impurities in the background is assumed to be 4. In the simulations, the carbon impurities in the background plasma mainly influence the carbon deposition on the surface but the re-deposition rates of the eroded particles are barely changed. So far the simulations only take into account the parallel flux ($\Gamma_{sur} = \Gamma_\parallel \cos\alpha$). Thus, while the background carbon

concentration increases, the amounts of the carbon deposition increases more significantly at the sides of the ML than that on the top surface because the impinging particle flux is larger there. The gross erosion rate does not change much with different carbon concentrations. Although a higher carbon concentration leads to more physical sputtering due to higher carbon physical sputtering yields bombarded by carbon impurities than by fuel ions, the number of chemically eroded particles is reduced due to the lower deuterium flux. Therefore, when the carbon concentration is very low and slightly increased, the increased physical sputtering rate and decreased chemical erosion rate make the gross erosion rates almost unchanged. Therefore, the net erosion rates decrease with the increase of carbon concentration at the sides of the ML due to the increase of background carbon deposition, but on the top surface of the ML, the rates remain relatively stable. Note that the first wall was full graphite tiles during the campaign when marked tiles were exposed, so the carbon concentration in the background plasma could be relatively high. But according to figure 5, too high a carbon concentration will make the net erosion rates lower than the lower limit of the experimental net erosion rate $0.028\,\mathrm{nm\,s^{-1}}$, therefore the value of ρ_c may not be higher than 2%.

As the perpendicular flux is not considered, the modelling results indicate that net deposition occurs on most of the top surface region as shown in figure 5. Simulations indicate that under the assumption of background carbon concentration $\rho_c = 2\%$, a higher particle flux on the top surface will turn the top surface from net deposition to net erosion. This is because in the case without perpendicular flux, the particle flux to the top surface is too small, which leads to low gross erosion rates and background carbon deposition. Thus, redeposition of carbon eroded from two sides of the ML plays an important role in the total deposition on the top surface ($\sim$40% of the total redeposited carbon for both divertor and limiter phases). According to the simulations, if no redeposition of carbon eroded from the two sides is taken into account, the top surface will be in the net erosion condition. Therefore, if the perpendicular flux is large enough, the top surface will turn from net deposition to net erosion due to the redeposition of the carbon eroded from two sides of the ML becoming less important. In the simulations, the additional flux bombarding the top surface due to perpendicular transport with shallow angles is implemented using a simple model according to equations (2) and (3). In the equations, $\Gamma_{||}$, c_s and α on each cell of the ML are calculated in accordance with the local plasma parameters, and L_f is the width of the ML top surface. However, the cross-field transport coefficient $D_\perp$ for the plasma adjacent to the absorbing wall of the surface is uncertain and anomalous. Therefore, different values of $D_\perp$ are assumed and studied in the simulation, as shown in figure 6. In this figure, the background carbon concentration $\rho_c = 1.8\%$ is assumed. Note that higher $D_\perp$ mainly increases the flux onto the top surface according to the relation of $\Gamma_\perp/\Gamma_\parallel \propto {D_\perp}^{1/2}$. When α is close to 90°, $\Gamma_\perp$ becomes the dominant part. Therefore the gross erosion can be significantly increased with increasing $D_\perp$. As the total carbon deposition on the top surface is mainly determined by the

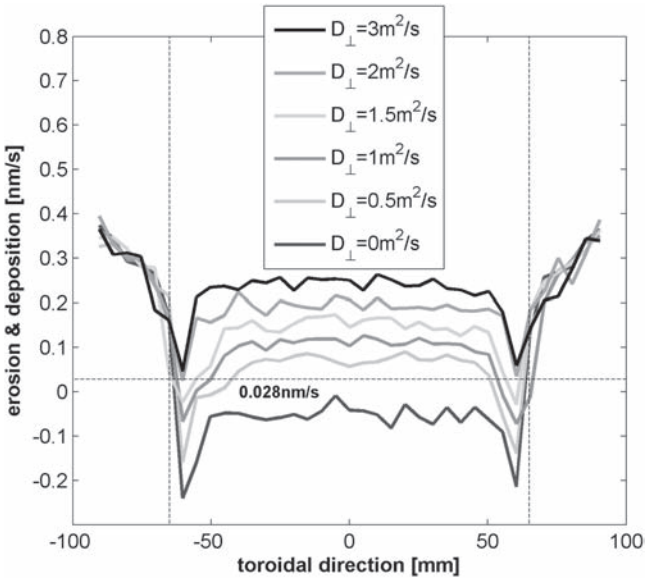

Figure 6. Modelled erosion and deposition distribution along the toroidal direction at the midplane (poloidal direction $z = 0$) of the movable limiter for different cross-field transport coefficients ($D_\perp$) on the top surface for $\rho_c = 1.8\%$.

background carbon concentration and the carbon eroded from the sides of the surface, which are approximately constant, the net erosion can be effectively enhanced by the increasing $D_\perp$. If $D_\perp$ is increased by $0.5\,\mathrm{m^2\,s^{-1}}$, the net erosion rate on the top surface will be increased by about $0.05\,\mathrm{nm\,s^{-1}}$. As shown in figure 6, when $D_\perp$ is larger than $2\,\mathrm{m^2\,s^{-1}}$, the net erosion rates on the top surface can reach the experimental lower limit $0.028\,\mathrm{nm\,s^{-1}}$. If $D_\perp$ is assumed to be $2\,\mathrm{m^2\,s^{-1}}$, the parameters for the ML experiment—$L_f = 0.065$ m, $T_e = 10$ eV, $c_s \approx 4 \times 10^4\,\mathrm{m\,s^{-1}}$ —give $\Gamma_\perp/\Gamma_\parallel \approx 0.1$, which is comparable to the previous experimental measured results of 0.05–0.1 in the DITE tokamak [8]. As an example, figures 7(a) and (b) show the distribution of parallel flux on the surface of the ML in the case of the limiter phase. Different colorbar ranges of the two figures are used for the purpose of distinguishing the side and middle parts of the limiter. Note that the flux on the top surface is asymmetric in the toroidal direction, because in the toroidal direction the plasma shape is curved but the limiter is flat, so the limiter cannot cut the flux tube perfectly. The total flux distribution including both parallel and perpendicular components on the top of the ML surface with $D_\perp = 2\,\mathrm{m^2\,s^{-1}}$ is shown in figure 7(c). Compared to figure 7(b), the perpendicular flux plays a dominant role in the top of the ML surface.

With the assumption of $\rho_c = 1.8\%$ and $D_\perp = 2\,\mathrm{m^2\,s^{-1}}$, the net erosion and deposition rate distribution at the midplane of the ML along the toroidal direction are shown in figure 8. The black solid line is the averaged net erosion rate according to the ratios of exposure time in the two phases. Note that the minimum net erosion rate is $0.03\,\mathrm{nm\,s^{-1}}$, which is slightly larger than $0.028\,\mathrm{nm\,s^{-1}}$. On the top surface of the ML, the net erosion rates for both the limiter phase and the divertor phase are around $0.2\,\mathrm{nm\,s^{-1}}$ and relatively homogeneous. But at the two sides of the limiter, the distributions

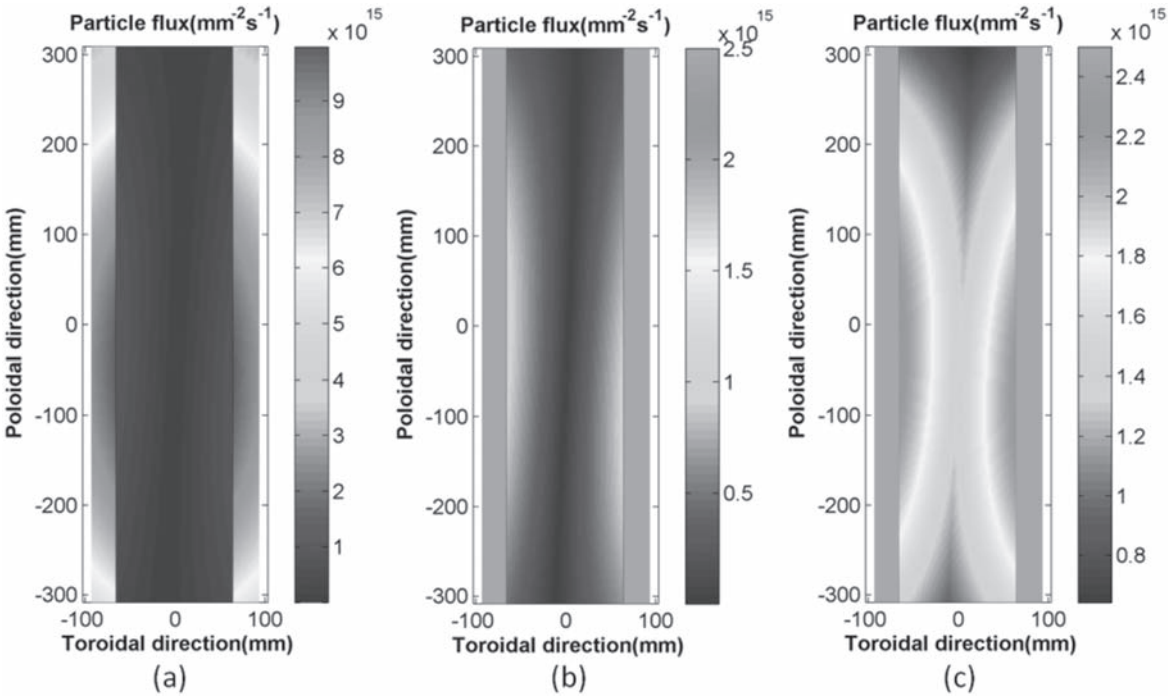

Figure 7. Distribution of particle flux to the movable limiter in limiter phase discharge. (a) and (b) Distribution of parallel flux with different colorbar ranges focusing on the sides and top surface respectively. (c) Distribution of total including both parallel and perpendicular fluxes with $D_\perp$ set to $2\ \mathrm{m^2\ s^{-1}}$.

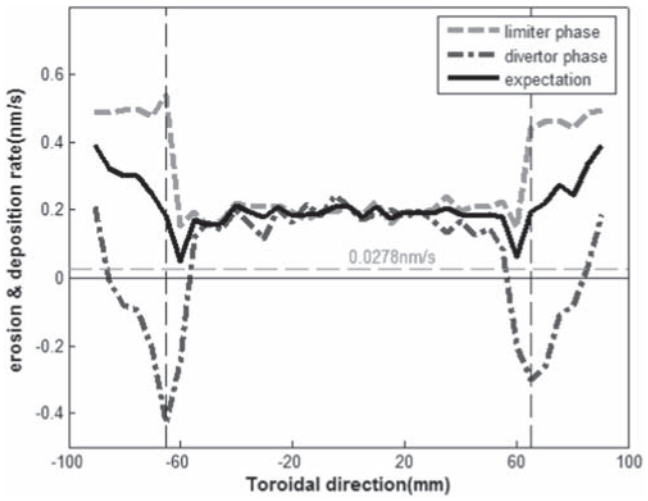

Figure 8. ERO modelled net erosion and deposition distribution for the movable limiter at the midplane (poloidal direction $z = 0$) along the toroidal direction. Red and blue dashed lines represent the limiter phase and divertor phase respectively. The black solid line represents the mathematical expectation according to the exposure time of the two phases, which is supposed to be the campaign averaged result.

are quite different for the two phases. Net erosion occurs for the limiter phase and the rate is about $0.5\ \mathrm{nm\ s^{-1}}$, whereas net deposition occurs for the divertor phase and the maximum deposition rate is around $0.4\ \mathrm{nm\ s^{-1}}$. One of the reasons is because of the different amounts of background carbon deposition due to the different plasma density, although the same carbon concentrations are assumed. Moreover the plasma temperature and density close to the movable limiter for the divertor phase are higher and decay much faster than those for the limiter phase. Thus the eroded materials in the divertor phase are easily forced back and redeposited locally to the surface due to strong friction by the background plasma. The simulation results indicate that the redeposition efficiency is 15.2% for the limiter phase while it is 51.7% for the divertor phase. Figure 9 shows the modeled averaged net erosion and deposition rates distribution for the whole limiter. It can be seen that there are net deposition regions on the bottom and top part of the limiter where no marked tiles exist. However, in the experiment no visible C deposition was found, and the C redeposition could not be measured quantitatively due to the graphite tile surface. At the midplane of the limiter, larger erosion rates occur at the two sides than at the top surface. Taking the maximum net erosion rate of $0.4\ \mathrm{nm\ s^{-1}}$, about $14.4\ \mu$m carbon could be eroded after 36 000 s discharges in the experiment campaign, which is much larger than the $1\ \mu$m carbon coating in the experiments.

5. Summary

The 3D Monte Carlo code ERO has been used to simulate carbon erosion, migration and re-deposition for the movable limiter in EAST. A model that takes into account the perpendicular flux of the shallow B field angle surface has been implemented into the code. The movable limiter geometry, 3D configurations of plasma parameters and electromagnetic field have been taken into account for both divertor phase and limiter phase discharges. Different uncertain parameters are studied to address their influence on the overall net erosion and deposition results. The background carbon concentration ρ_c

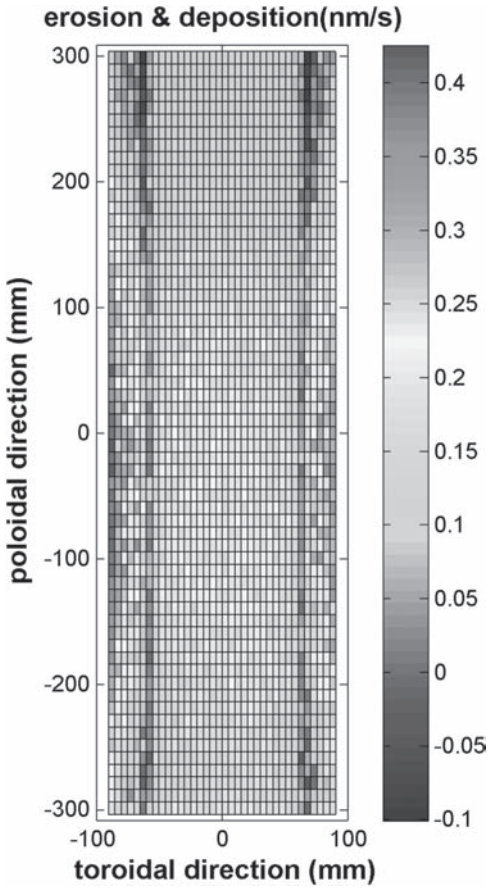

Figure 9. ERO modelled net erosion and deposition distribution for the movable limiter.

mainly influences the net erosion and deposition profiles of the two sides of the ML, which have been shaped with angles of 15°, while the cross field coefficients $D_\perp$ mostly change the profiles on the top surface. Comparing with the experiment results, ρ_c in the simulation has to be lower than 2% and $D_\perp$ may not be higher than $2\,m^2\,s^{-1}$. With the assumptions of $\rho_c = 1.8\%$, $D_\perp = 2\,m^2\,s^{-1}$, net erosion occurs at the midplane of the ML with the maximum rate of $0.4\,nm\,s^{-1}$ and minimum rate of $0.03\,nm\,s^{-1}$, which is higher than the lowest experimental measurement value $0.028\,nm\,s^{-1}$. The net erosion and deposition distributions separately for the limiter phase and the divertor phase have also be obtained and studied. However, only two typical shots are used to modell the campaign averaged results. There are still many uncertainties during the campaign which have not been considered in the simulation, such as wall conditioning, edge localized modes (ELMs) and other transient events, etc. Therefore, more refined experiments of material exposed to plasma discharges with a single plasma condition need to be carried out to compare with the modelling results.

Acknowledgments

This work has been supported by the National Magnetic Confinement Fusion Science Program of China (Nos. 2013GB107004 and 2013GB105003), National Natural Science Foundation of China (Nos. 11375010, 11675218 and 11005125), and the Sino-German Center for Research Promotion under Contract No. GZ769.

References

[1] Roth J *et al* 2009 *J. Nucl. Mater.* **390–391** 1
[2] Shimida M *et al* 2007 *Nucl. Fusion* **47** S1
[3] Federici G *et al* 2001 *Nucl. Fusion* **41** 1967
[4] Kobayashi M *et al* 2007 *Nucl. Fusion* **47** 61
[5] Pitts R A *et al* 2011 *J. Nucl. Mater.* **415** S957
[6] Carpentier S *et al* 2011 *J. Nucl. Mater.* **415** S165
[7] Borodin D *et al* 2011 *Phys. Scr.* **T145** 014008
[8] Matthews G F *et al* 1990 *Plasma Phys. Control. Fusion* **32** 1301
[9] Li Q *et al* 2010 *Fusion Eng. Des.* **85** 126
[10] Matthews G F *et al* 2007 *Nucl. Fusion* **31** 1383
[11] Arnoux G *et al* 2013 *Nucl. Fusion* **53** 073016
[12] Theilhaber K and Birdsall C K 1989 *Phys. Fluids* B **1** 2260
[13] Tskhakay D and Kuhn S 2003 *J. Nucl. Mater.* **313–316** 1119
[14] Stangeby P C, Pitcher C S and Elder J D 1992 *Nucl. Fusion* **32** 2079
[15] Stangeby P C 2012 *Nucl. Fusion* **52** 083012
[16] Kirschner A *et al* 2000 *Nucl. Fusion* **40** 989
[17] Guo H Y *et al* 2011 *J. Nucl. Mater.* **415** S369
[18] Cao L and Song Y T 2011 *Fusion Eng. Des.* **86** 1603
[19] Chen J L *et al* 2004 *Phys. Scr.* **T111** 173
[20] Qian J P *et al* 2009 *J. Plasma Phys* **75** 337
[21] Abramov V A *et al* 1989 *J. Nucl. Mater.* **162–164** 462
[22] Roth J *et al* 2005 *J. Nucl. Mater.* **337–339** 970
[23] Pospieszczyk A *et al* 1997 *J. Nucl. Mater.* **241–243** 833
[24] Brezinsek S *et al* 2007 *J. Nucl. Mater.* **363–365** 1119
[25] Ding R *et al* 2009 *Plasma Phys. Control. Fusion* **51** 055019
[26] Ding R *et al* 2010 *Plasma Phys. Control. Fusion* **52** 045005